UC Berkeley
UC Berkeley Previously Published Works

Title
Asymmetric Electrical Double Layer Charging in Ionomers under Pure Water

Permalink
https://escholarship.org/uc/item/5zc0f3f7

Authors
Kang, Yunseok
Roncoroni, Fabrice
Pendergast, Andrew D
et al.

Publication Date
2026-10-02

DOI
10.26434/chemrxiv.15009777/v1

Copyright Information
This work is made available under the terms of a Creative Commons Attribution License, available at https://creativecommons.org/licenses/by/4.0/

eScholarship.org Powered by the California Digital Library
University of California

2 October 2026

Asymmetric Electrical Double Layer Charging in Ionomers under Pure Water

Yunseok Kang[1,2,3,4], Fabrice Roncoroni[5], Andrew D. Pendergast[1,2], Wenbo Zhang[1,2], Mei-Chen Kuo[6], Ahmet Kusoglu[2], David Prendergast[5], Andrew M. Herring[6], Jungki Ryu[3,4,7], Shannon W. Boettcher[1,2]

1. Department of Chemical and Biomolecular Engineering and Department of Chemistry, California
2. Energy Technologies & Systems Division, Lawrence Berkeley National Laboratory
3. School of Energy and Chemical Engineering, Ulsan National Institute of Science and Technology (UNIST
4. Ulsan National Institute of Science and Technology (UNIST
5. Molecular Foundry, Lawrence Berkeley National Laboratory
6. Department of Chemical and Biological Engineering, Colorado School of Mines
7. Graduate School of Carbon Neutrality, Ulsan National Institute of Science and Technology (UNIST

Abstract

Electrode interfaces with ionic polymers (ionomers) create local microenvironments in membrane electrolysis and other applications, yet the formation and dynamics of electrical double layers (EDLs) at ionomer|electrode interfaces are incompletely understood. Unlike traditional aqueous electrolytes with both mobile cations and anions, ionomer interfaces couple mobile counterion motion to the slower response of tethered polymer-backbone ionic groups. Studying these solid|ionomer interfaces, with pure water feed as in many technology applications, is more difficult than with conventional electrolytes due to the lack of a liquid supporting electrolyte for simple integration of counter and reference electrodes. Here, we use a membrane-electrode-assembly-inspired architecture with a lateral ionomer strip and a salt-bridged reference electrode to independently track anodic and cathodic potentials while sweeping the voltage between the two Pt-solid|ionomer interfaces in pure water. We quantify electrode-resolved non-faradaic charging and show that fixed polymer charges and mobile counterions contribute differently to interfacial capacitance. In anion-exchange ionomers, mobile Cl- responds rapidly, whereas fixed quaternary ammonium groups relax more slowly, producing a capacitance asymmetry. This asymmetry weakens when sufficient time is allowed for relaxation and is suppressed by supporting electrolyte. When Nafion cation-exchange ionomer is used instead, the results show a reversal in the sign of the asymmetry. Supporting molecular dynamics simulations establish coupled counterion motion and tethered-charge relaxation as governing features of pure-water ionomer EDLs. The work thus provides a framework for studying and ultimately designing ionomer microenvironments for membrane

Posted on 2 October 2026 — CC-BY-NC-ND 4.0 — This is a preprint and has not been peer reviewed. Data may be preliminary. —
https://doi.org/10.26434/chemrxiv.15009777/v1

electrolysis and other applications. The Bigger Picture Pure-water-fed membrane electrolyzers rely on ionomers to carry charge to catalyst surfaces. Unlike soluble liquid electrolytes, ionomers contain mobile counterions and oppositely charged groups fixed to a polymer chain. The details of how these charges form electrical double layers under positive and negative polarization are not fully understood. We developed a model cell with a solid ionomer electrolyte that senses each electrode potential separately during cell operation. The measurements show asymmetric, time-dependent charging in pure water, with mobile counterions responding more rapidly than polymer-bound charge. Added electrolytes suppress this charging-rate imbalance; reversing the ionomer charge sign also reverses the asymmetry of the charging response, and a custom-synthesized more-flexible polymer backbone reduces the rate dependence of the apparent capacitance. The work here shows how the ionomer is an active part of the electrochemical interface, in addition to an ion conductor in the bulk. The platform and fundamental principles developed here are relevant to water electrolyzers, fuel cells, and other membrane-based electrochemical devices.

Keywords

ionomer, electrical double layer, pure-water electrolysis, interfacial capacitance, ionomer-potential sensing

Posted on 2 October 2026 — CC-BY-NC-ND 4.0 — This is a preprint and has not been peer reviewed. Data may be preliminary. — https://doi.org/10.26434/chemrxiv.15009777/v1

Asymmetric Electrical Double Layer Charging in Ionomers under Pure Water

Yunseok Kang[1,2,3,4], *Fabrice Roncoroni*[5], *Andrew D. Pendergast*[1,2], *Wenbo Zhang*[1,2], *Mei-Chen Kuo*[6], *Ahmet Kusoglu*[2], *David Prendergast*[5], *Andrew M. Herring*[6], *Jungki Ryu*[3,4,7*], *Shannon W. Boettcher*[1,2,8*]

[1]Department of Chemical and Biomolecular Engineering and Department of Chemistry, University of California, Berkeley, California 94720, United States

[2]Energy Technologies & Systems Division, Lawrence Berkeley National Laboratory, Berkeley, CA 94720, USA

[3]School of Energy and Chemical Engineering, Ulsan National Institute of Science and Technology (UNIST), Ulsan 44919, Republic of Korea

[4]Emergent Hydrogen Technology R&D Center, Ulsan National Institute of Science and Technology (UNIST), Ulsan 44919, Republic of Korea

[5]The Molecular Foundry, Lawrence Berkeley National Laboratory, Berkeley, California 94720, USA

[6]Department of Chemical and Biological Engineering, Colorado School of Mines, Golden, Colorado 80401, USA

[7]Graduate School of Carbon Neutrality, Ulsan National Institute of Science and Technology (UNIST), Ulsan 44919, Republic of Korea

[8]Lead contact

Keywords: ionomer; electrical double layer; pure-water electrolysis; interfacial capacitance; ionomer-potential sensing

[*]Correspondence: jryu@unist.ac.kr (J.R.), boettcher@berkeley.edu (S.W.B.)

Abstract

Electrode interfaces with ionic polymers (ionomers) create local microenvironments in membrane electrolysis and other applications, yet the formation and dynamics of electrical double layers (EDLs) at ionomer|electrode interfaces are incompletely understood. Unlike traditional aqueous electrolytes with both mobile cations and anions, ionomer interfaces couple mobile counterion motion to the slower response of tethered polymer-backbone ionic groups. Studying these solid|ionomer interfaces, with pure water feed as in many technology applications, is more difficult than with conventional electrolytes due to the lack of a liquid supporting electrolyte for simple integration of counter and reference electrodes. Here, we use a membrane-electrode-assembly-inspired architecture with a lateral ionomer strip and a salt-bridged reference electrode to independently track anodic and cathodic potentials while sweeping the voltage between the two Pt-solid|ionomer interfaces in pure water. We quantify electrode-resolved non-faradaic charging and show that fixed polymer charges and mobile counterions contribute differently to interfacial capacitance. In anion-exchange ionomers, mobile Cl^- responds rapidly, whereas fixed quaternary ammonium groups relax more slowly, producing a capacitance asymmetry. This asymmetry weakens when sufficient time is allowed for relaxation and is suppressed by supporting electrolyte. When Nafion cation-exchange ionomer is used instead, the results show a reversal in the sign of the asymmetry. Supporting molecular dynamics simulations establish coupled counterion motion and tethered-charge relaxation as governing features of pure-water ionomer EDLs. The work thus provides a framework for studying and ultimately designing ionomer microenvironments for membrane electrolysis and other applications.

The Bigger Picture

Pure-water-fed membrane electrolyzers rely on ionomers to carry charge to catalyst surfaces. Unlike soluble liquid electrolytes, ionomers contain mobile counterions and oppositely charged groups fixed to a polymer chain. The details of how these charges form electrical double layers under positive and negative polarization are not fully understood.

We developed a model cell with a solid ionomer electrolyte that senses each electrode potential separately during cell operation. The measurements show asymmetric, time-dependent charging in pure water, with mobile counterions responding more rapidly than polymer-bound charge. Added electrolytes suppress this charging-rate imbalance; reversing the ionomer charge sign also reverses the asymmetry of the charging response, and a custom-synthesized more-flexible polymer backbone reduces the rate dependence of the apparent capacitance. The work here shows how the ionomer is an active part of the electrochemical interface, in addition to an ion conductor in the bulk. The platform and fundamental principles developed here are relevant to water electrolyzers, fuel cells, and other membrane-based electrochemical devices.

1. Introduction

Electrical double layers (EDLs) are ubiquitous at biological membranes,[1,2] mineral–aqueous interfaces,[3,4] and electrode–electrolyte interfaces.[5,6] The charge organization and electric potential distribution in these electrochemical interfaces are shaped by ion concentration, size, and other ion-specific effects[7,8] including solvation structure[9-11] and field-induced solvent orientation.[12,13] The molecular electrolyte and interface properties ultimately determine how any interfacial potential drop distributes and control the apparent interfacial capacitance and its frequency dependence.[14] These concepts have been developed primarily for liquid electrolytes containing a supporting salt, where mobile anions and cations both respond to interfacial fields and compose the typical compact- and diffuse-layer Gouy–Chapman–Stern model descriptions as a useful approximation.[5,8,15]

For solid electrolytes, e.g., ionomer membranes with mobile counterions and backbone-tethered ionic groups, this model requires modification.[16-18] Ionomers comprise repeated ionic units connected along chains with varying segmental dynamics affecting ion dissociation and mobility.[16,17] Unlike solvated ions, ionomer polarization proceeds through segmental rotation and constrained relaxation rather than unrestricted translational motion.[19,20]

Understanding ionomer-based electrochemical double layers is important for interpreting interfacial charging in typical pure-water-fed proton-exchange-membrane and hydroxide-exchange membrane electrolyzers, membrane-based fuel cells, and related electrochemical devices.[21-27] These interfaces, which lack soluble supporting electrolyte, are distinct from conventional salt-containing electrolytes and complicate direct experimental measurement of the potential drop and apparent capacitance at each ionomer–electrode interface.[20] In this regime, counterions serve as the primary mobile charges, whereas the ionomer charge remains attached to the polymer backbone with limited mobility.[17] Therefore, interfacial

charging can no longer be assessed directly using descriptions developed for liquid electrolytes dominated by freely mobile ions. In such cases, the ionomer functions as a solid electrolyte in which electrode charge is compensated by counterion redistribution, interfacial-water polarization, and relaxation of polymeric charges, rather than by a diffuse layer of mobile salt ions.[18,28-31]

Here, we report a model system that enables electrode-resolved quantification of anodic and cathodic catalyst–ionomer interfaces during two-electrode operation in pure water. The system consists of an ionomer membrane sandwiched between two planar metal electrodes with a reference electrode integrated through a membrane tab and electrolyte bridge. By tracking anodic and cathodic potentials relative to the reference electrode, this platform enables quantification of interfacial capacitive charging at each electrode through time-dependent cyclic voltammetry and frequency-dependent impedance spectroscopy. Although related reference-based strategies have been used in full-cell electrochemical devices,[32-34] the present model platform minimizes the transport and ohmic heterogeneity of practical porous-electrode-supported systems, enabling more-direct diagnosis of catalyst–ionomer interfacial charging under pure-water conditions.

Using anion- and cation-exchange ionomers, we quantify anodic and cathodic capacitance contributions in pure water and upon addition of a supporting electrolyte, revealing asymmetric capacitive responses that distinguish rapid counterion accumulation from the slower charging of polymer-tethered ionic groups. Combined with constant-potential molecular dynamics (MD) simulations, these data further show that pure-water ionomer EDLs are governed by coupled ionic screening and interfacial water polarization, which together shape voltage partitioning and capacitance asymmetry. These findings establish a framework for understanding and quantifying EDL formation and response at

ionomer–electrode interfaces in pure-water microenvironments and provide a basis for engineering catalyst–ionomer microenvironments in ionomer-based electrochemical devices by linking the apparent interfacial capacitance to the local potential drop and the time scales for ionomer screening.

2. Results and Discussion

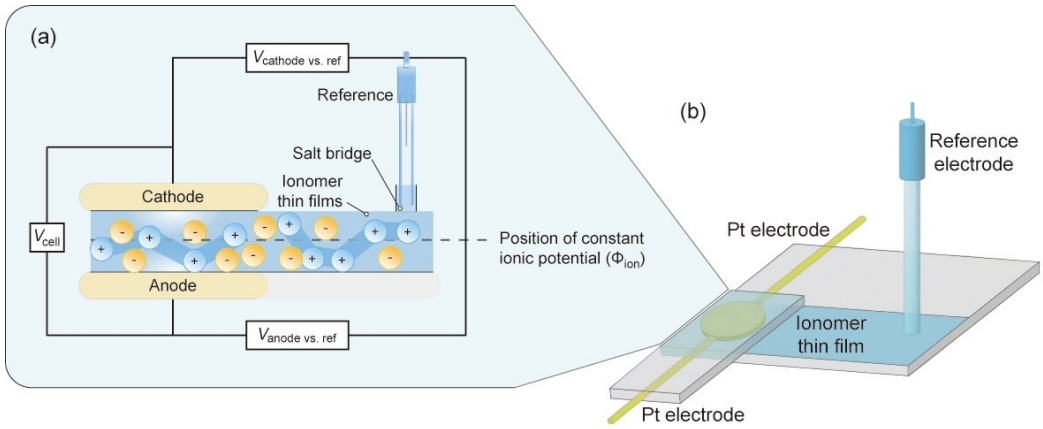


Figure 1. **Ionomer-potential-sensing platform for electrode-resolved measurements in a pure-water microenvironment. (a)** The ionomer thin film is confined between the two Pt electrodes and functions as a solid electrolyte, whereas the laterally extended strip carries negligible ionic current and therefore remains at an approximately uniform ionomer electrostatic potential. This configuration enables independent determination of the anodic and cathodic potentials (V_{anode} and $V_{cathode}$ vs. reference) during operation, thereby allowing electrode-resolved analysis of interfacial charging in pure water. **(b)** Schematic of the Pt|ionomer|Pt sandwich model cell used to record the anode and cathode potentials during cell-voltage sweeps in pure water. A laterally extended ionomer strip is coupled to a salt-bridged reference electrode, enabling local potential sensing without introducing supporting electrolyte into the measurement region.

2.1 Resolving Electrode-Specific Charging in Pure-Water Ionomer Microenvironments

To probe electrochemical behavior within ionomer microenvironments without soluble supporting electrolyte (e.g., in pure water), we fabricated planar Pt thin-film electrodes on glass slides by electron-beam evaporation (with Ti adhesion layer) and used them as model electrode surfaces (**Fig. 1a**). Pt was chosen as the electrode material because it is a standard catalyst in water electrolysis and has well-characterized interfacial chemistry.[35-

[37] Although Pt forms surface oxides under sufficiently positive polarization, we report the extracted capacitance as apparent interfacial values. PiperION was spray-coated onto the active Pt region of each electrode under the same conditions, giving dry ionomer films of ~9 μm thickness (**Fig. S1**). On one electrode substrate, the ionomer coating was extended laterally beyond the Pt/Pt overlap region onto the glass slide to form a continuous ionomer-potential sensing strip. The two coated electrodes were then assembled face-to-face so that the active Pt regions were separated by the sprayed ionomer film, while the extended strip remained outside the through-plane current path. A salt bridge connected this strip to a reference electrode, providing a probe of the local ionomer potential (like a Luggin capillary) without introducing supporting electrolyte into the active region (**Fig. S2**).[38] Because the lateral strip carries negligible ionic current, the in-plane potential drop along the strip is small compared with the through-plane potential drop across the active Pt|ionomer|Pt region. The reference electrode is therefore expected to report the ionomer potential during cell-voltage sweeps (**Fig. 1b**).

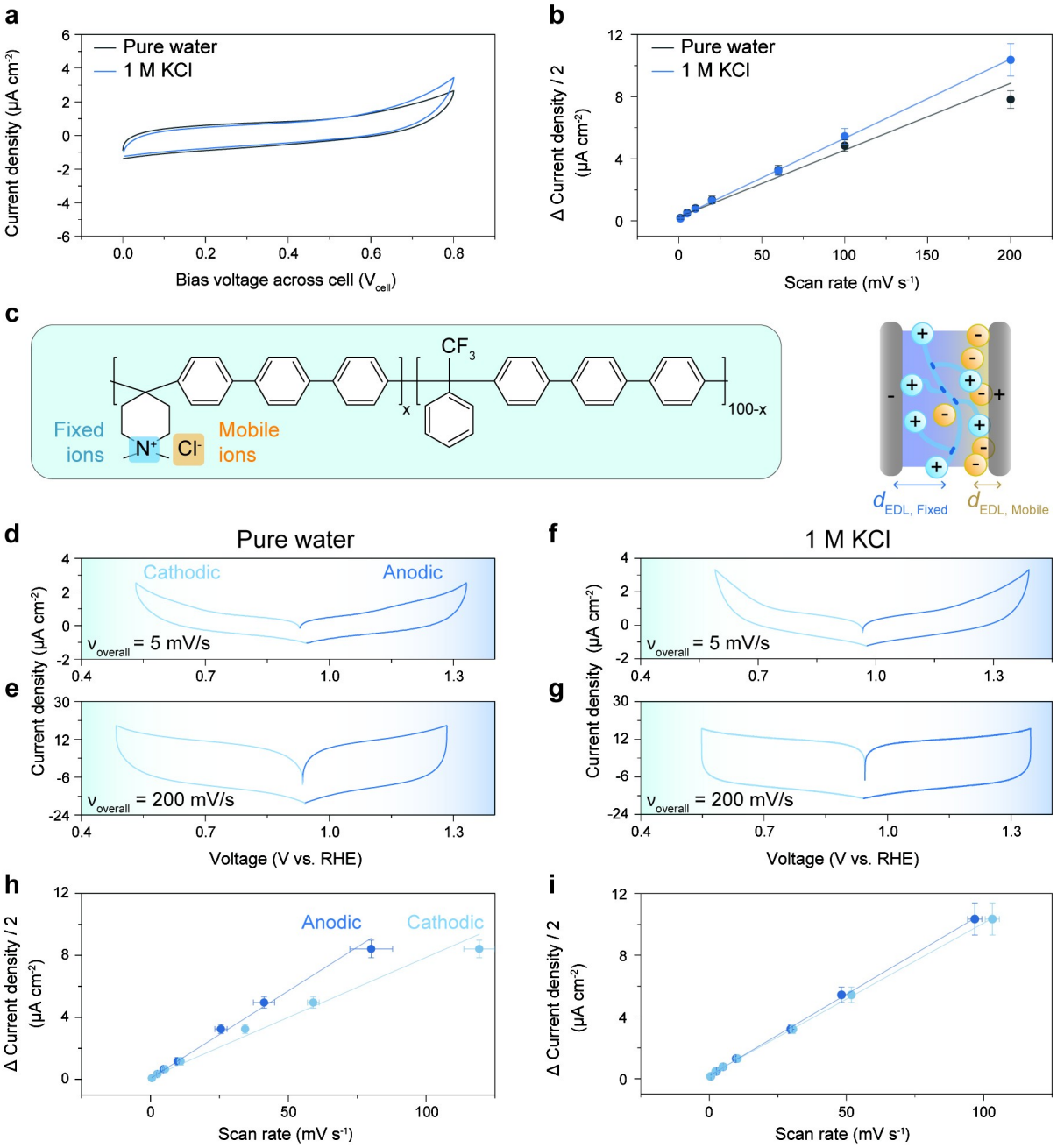


Figure 2. Double-layer charging in pure water versus supporting electrolyte. (a) Overall cell voltammetry of the Pt|PiperION|Pt ionomer-sensing cell in pure water and 1.0 M KCl, showing the non-faradaic response as a function of cell bias. **(b)** Current density–scan rate dependence at 0.40 V_{cell} extracted from (a), used to determine the apparent double-layer capacitance for each environment. **(c)** Chemical structure of PiperION, highlighting fixed quaternary ammonium (QA^+) sites and mobile Cl^- counterions, together with a schematic of ionomer-mediated EDL formation at the two Pt electrodes. **(d, e)** Anodic and cathodic voltammograms obtained by plotting the measured cell current against V_{anode} or $V_{cathode}$, respectively, at cell scan rates of (d) 5 mV s^{-1} and (e) 200 mV s^{-1}, showing the emergence of scan-rate-dependent asymmetry between the two interfaces. In this experiment, the total potential across both electrodes is swept at the indicated scan rate. As the current is passed, the potential distributes across the two electrodes with different capacitances at different rates as represented by

the asymmetry. **(f, g)** Corresponding anodic and cathodic CVs in 1.0 M KCl at (f) 5 mV s^{-1} and (g) 200 mV s^{-1}, where the presence of supporting electrolyte ions yields nearly symmetric charging behavior over the same potential window. We also measured 400, 600, 800, and 1000 mV/s, and included these data in the model fit. **(h)** Anodic and cathodic current densities at 0.40 V_{cell} in pure water plotted versus scan rate, extracted from (d, e), and used to obtain separate double-layer capacitances for each electrode. **(i)** Scan-rate-dependent charging current plots for a device in 1.0 M KCl, showing linear and nearly identical anodic and cathodic responses.

2.2 Pure Water Exposes Time-Dependent Asymmetric Double-Layer Charging in Anion-Exchange Ionomers

Electrochemical measurements of interfacial charging in an anion-exchange ionomer (AEI) film (here, PiperION) were conducted under both pure-water and supporting-electrolyte conditions using the new potential-sensing platform. The cell voltage was swept between the two Pt electrodes while V_{anode} and $V_{cathode}$ were measured relative to the integrated reference electrode potential. Supplementary Video 1 shows a representative pure-water scan at 200 mV s^{-1}, with the same measured cell current plotted against V_{cell}, V_{anode}, and $V_{cathode}$ as the scan proceeds. This approach overcomes the voltage-partitioning limitation of conventional two-electrode measurements and enables quantitative separation of the individual electrode contributions during operation (**Fig. S2**).

Cyclic voltammetry (CV) was first performed in a two-electrode mode with scan rates from 1 to 200 mV s^{-1} over 0.0–0.8 V to characterize interfacial charging. From linear fits of capacitive current versus scan rate, the apparent double-layer capacitance (C_{dl}) was 42 ± 3 μF cm^{-2} in pure water and 49 ± 3 μF cm^{-2} in 1.0 M KCl, corresponding to a modest ~16% increase upon introduction of supporting electrolyte (**Fig. 2a, b**). As a benchmark, measurements in a conventional three-electrode cell yielded single-electrode capacitances of 70.1 and 89.0 μF cm^{-2} in 0.10 M and 1.0 M KCl, respectively (**Fig. S3**). A simple series-circuit estimate, assuming two identical Pt/electrolyte interfaces in such an electrolyte, would

therefore give ~35 and 45 μF cm^{-2}, respectively, bracketing the 42 ± 3 μF cm^{-2} measured in the two-electrode device platform with pure water (most co-ions from electrolyte are excluded from the ionomer by Donnan effects).

To determine whether the pure-water response of 42 ± 3 μF cm^{-2} could be limited by the available mobile charge in the ionomer, we performed a simple charge-balance estimate. The exchangeable Cl^- inventory in the ~9 μm PiperION film exceeds the charge required to account for the measured capacitive current by four orders of magnitude ($N_{counter} \sim 1.4 \times 10^{18}$ vs. $N_{EDL} \sim 1.4 \times 10^{14}$; **Supplementary Note 1**), indicating that the response is limited not by counterion availability but by how mobile ions and ionomer-bound charge distributions reorganize near the polarized interfaces.

Under pure-water conditions, the overall cell CV response became nonlinear at a scan rate of 200 mV s^{-1}, with a decrease in measured capacitance at faster sweeps (**Fig. 2b**). At 200 mV s^{-1} the extracted capacitive current falls below the linear fit by 0.38 μA cm^{-2}, reflecting the inability of the hydrated ionomer to fully reorganize on the relevant time scale (**Fig. S4**). In contrast, when a supporting electrolyte is present, the response remains linear, deviating by only 0.05 μA cm^{-2} from the extrapolated trendline.

Finite-rate ion transport can make CV-derived capacitance dependent on scan rate even at a planar interface.[39] We next calculated the scan-rate-dependent apparent capacitance, $C_{app}(\nu)$, from the forward-reverse CV branch separation rather than assigning a single C_{dl} value to the full scan-rate range.[40] To parameterize this behavior with the minimum number of fitted parameters, we represented the interfacial charging as the sum of a fast component and a slower relaxing component, which yields (see Supporting Information) a scan-rate-dependent capacitance of $C_{app}(\nu) = C_\infty + \frac{C_1}{1+(\pi \nu \tau_{app}/\Delta E)^2}$. For the ion-exchange ionomers, the

fast response is expected to be dominated by rapid mobile-counterion redistribution together with fast solvent and electronic polarization, whereas the slower response would include reorganization of the polymer-tethered fixed-charge species.

The fits yielded C_1 = 31.0 and 32.9 μF cm^{-2} in pure water and 1.0 M KCl, respectively, while the fitted high-rate limits, C_∞, were 32.9 and 40.7 μF cm^{-2} (**Fig. S5a**). The corresponding apparent relaxation times, τ_{app}, were 2.6 s in pure water and 0.6 s in 1.0 M KCl (**Fig. S5b**). Within this model, C_∞ represents the capacitance retained in the fitted high-rate limit, whereas τ_{app} characterizes the response time of the slow component C_1. The smaller value in KCl shifts the attenuation of this contribution to higher scan rates.

To determine how the overall cell response was partitioned between the two interfaces, we recorded V_{anode} and $V_{cathode}$ simultaneously against the integrated reference during the same cell-voltage sweep (**Figs. 2c–2i**). Although the cell was operated in a two-electrode mode, the integrated reference allowed us to continuously track the anode and cathode potentials during the measurement, thereby providing three-electrode-like access to the individual electrode responses (**Fig. S6**). Because the two ionomer–electrode interfaces are connected in series, the applied cell-voltage sweep is divided between V_{anode} and $V_{cathode}$ while the same current passes through both interfaces. For a representative pure-water scan at 200 mV s^{-1}, linear fits to the increasing and decreasing portions of both potential traces gave $R^2 > 0.99$ (**Fig. S7**). For each interface, the local scan rate was taken as the mean absolute slope of the increasing and decreasing sweeps. The agreement between the sum of the fitted average local sweep rates and the applied cell scan rate therefore provides an internal check on the potential-sensing analysis (**Fig. S8**). Under pure-water conditions at a scan rate of 5 mV s^{-1}, the reference-tracked anodic and cathodic CVs corresponded to local average sweep rates of 2.46 and 2.52 mV s^{-1}, respectively (**Fig. 2d** and **Fig. S6**). At a high applied cell scan

rate of 200 mV s^{-1}, a pronounced asymmetry emerged, with an apparent capacitance of 80 ± 8 μF cm^{-2} at the cathode and 120 ± 6 μF cm^{-2} at the anode (**Fig. 2h**), which in series would give 48 μF cm^{-2}, consistent with the measurements above. This divergence indicates that the two interfaces no longer respond on the same time scale under rapid polarization. The anode interface exhibited a larger apparent capacitance, consistent with faster accumulation of the mobile Cl^- counterions, whereas the cathodic interface exhibited a smaller apparent capacitance, consistent with slower reorganization under changing bias of quaternary ammonium (QA^+) groups constrained within the ionomer matrix (**Fig. 2h**). Under these finite sweep-rate conditions, the limited segmental rearrangement of the hydrated ionomer is expected to hinder complete double-layer reorganization at the cathodic side, producing a time-dependent asymmetry in the apparent capacitance.

We then applied the same electrode-resolved analysis to the 1.0 M KCl data to determine how dissolved supporting ions affect the charging imbalance observed in the pure-water system. If the asymmetry in pure water indeed reflects rate-limited charging by the ionomer-bound species, these dissolved ions should reduce the imbalance by redistributing more rapidly under applied bias. Upon addition of 1.0 M KCl, the asymmetry was suppressed. At 200 mV s^{-1}, the anodic and cathodic capacitances were similar at 104 ± 3 and 96 ± 3 μF cm^{-2}, respectively, yielding nearly symmetric interfacial responses (**Fig. 2i**). This result supports the interpretation that, in pure water, the absence of freely mobile ions imposes a kinetic limitation on interfacial charging, whereas with electrolyte solutions, the faster redistribution of dissolved ions compensates for that limitation.

We then repeated the electrode-resolved analysis in additional chloride electrolytes, including LiCl, NaCl, and $CaCl_2$, and compared the anodic and cathodic apparent capacitances through the ratio, $C_{anode}/C_{cathode}$, at both low (1.0 mV s^{-1}) and high (200 mV s^{-1})

scan rates (**Fig. S9a**). At 1.0 mV s^{-1}, all chloride electrolytes gave ratios near unity. At 200 mV s^{-1}, where the pure-water ionomer cell showed a larger asymmetry, the chloride electrolytes kept $C_{anode}/C_{cathode}$ within ~10% of unity. LiCl showed the largest residual high-rate asymmetry and the highest high-frequency resistance (R_{HFR}, see below), whereas NaCl and KCl showed more symmetric charging, suggesting that stronger Li^+ hydration limits cation redistribution within the ionomer at high scan rates. This response indicates that the reduced asymmetry is not unique to KCl, but occurs generally when dissolved ions are available to participate in interfacial screening during the voltage sweep.

We also compared the electrode-resolved capacitance ratios with the $R_{HFR,}$ extracted from the two-electrode EIS fits under the same electrolyte conditions (**Fig. S9b)**. At the capacitive current densities used here, the corresponding $i \cdot R_{HFR}$ drops were sub-millivolt, and the estimated $R_{HFR}C$ time constants were much shorter than the voltage-sweep time. Thus, the measured capacitance ratios are not controlled by uncompensated high-frequency resistance and cell capacitance.

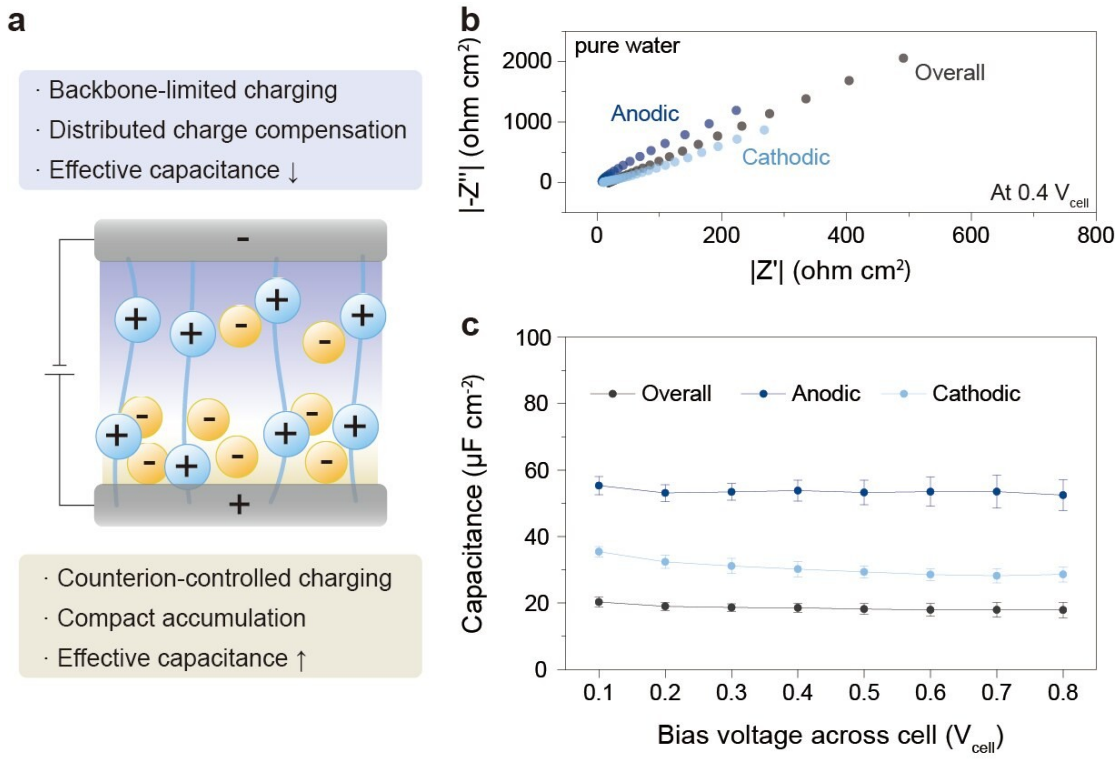


Figure 3. EIS analysis of asymmetric interfacial polarization using the ionomer-sensing platform. (a) Conceptual schematic of the asymmetric charging response, contrasting mobile counterion-controlled and backbone-limited interfacial polarization. Mobile Cl^- counterions respond more readily to the oscillatory perturbation and contribute a larger effective capacitance within the measurement window. In contrast, the backbone-coupled fixed-charge response is more distributed and relaxes more slowly, yielding a smaller effective capacitance within the same frequency window. **(b)** Representative Nyquist plots acquired at 0.40 V_{cell} and used to deconvolute the overall, anodic, and cathodic impedance responses. Impedance spectra were fit with a Randles-type equivalent circuit including a constant-phase element (CPE), and the fitted parameters were converted to effective capacitance using the Brug correction. **(c)** Bias-dependent Brug-corrected effective capacitances[41,42] for the overall cell and the separately extracted anodic and cathodic branches. Under pure-water conditions, the anodic capacitance exceeds the cathodic capacitance across the examined bias range, consistent with more readily established counterion-mediated polarization at the anodic interface and a more limited fixed-charge-associated response at the cathodic interface.

Following the CV analysis in the time domain, electrochemical impedance spectroscopy (EIS) was performed using the same ionomer-sensing platform (**Fig. 3b**). The impedance spectra collected at each applied bias were fitted with a Randles-type equivalent circuit containing a constant-phase element (CPE) to account for non-ideal interfacial

polarization, and the fitted CPE parameters were converted to effective capacitances using the Brug relation (**Fig. S10**). Because EIS measurements sample the electrochemical response over a defined frequency window, the extracted capacitance reflects the charge that can reorganize on the corresponding time scales. In the anion-exchange ionomer, mobile Cl^- redistribution provides a faster screening pathway at the anodic interface, whereas cathodic screening involving polymer-tethered QA^+ groups requires local side-chain and segmental relaxation within the hydrated ionomer.

Under pure-water conditions, the Brug-corrected capacitances reproduced the polarity of the asymmetry observed by CV (**Fig. 3c**). Across the examined bias range, the anodic capacitance was larger than the cathodic capacitance by a factor of ~1.9 on average. We interpret this frequency-domain asymmetry as a difference in the polarization accessible within the EIS time scale. Addition of 1.0 M KCl decreased the anodic/cathodic capacitance difference (**Fig. S11**), consistent with dissolved ions providing faster charge-compensation pathways at both interfaces.

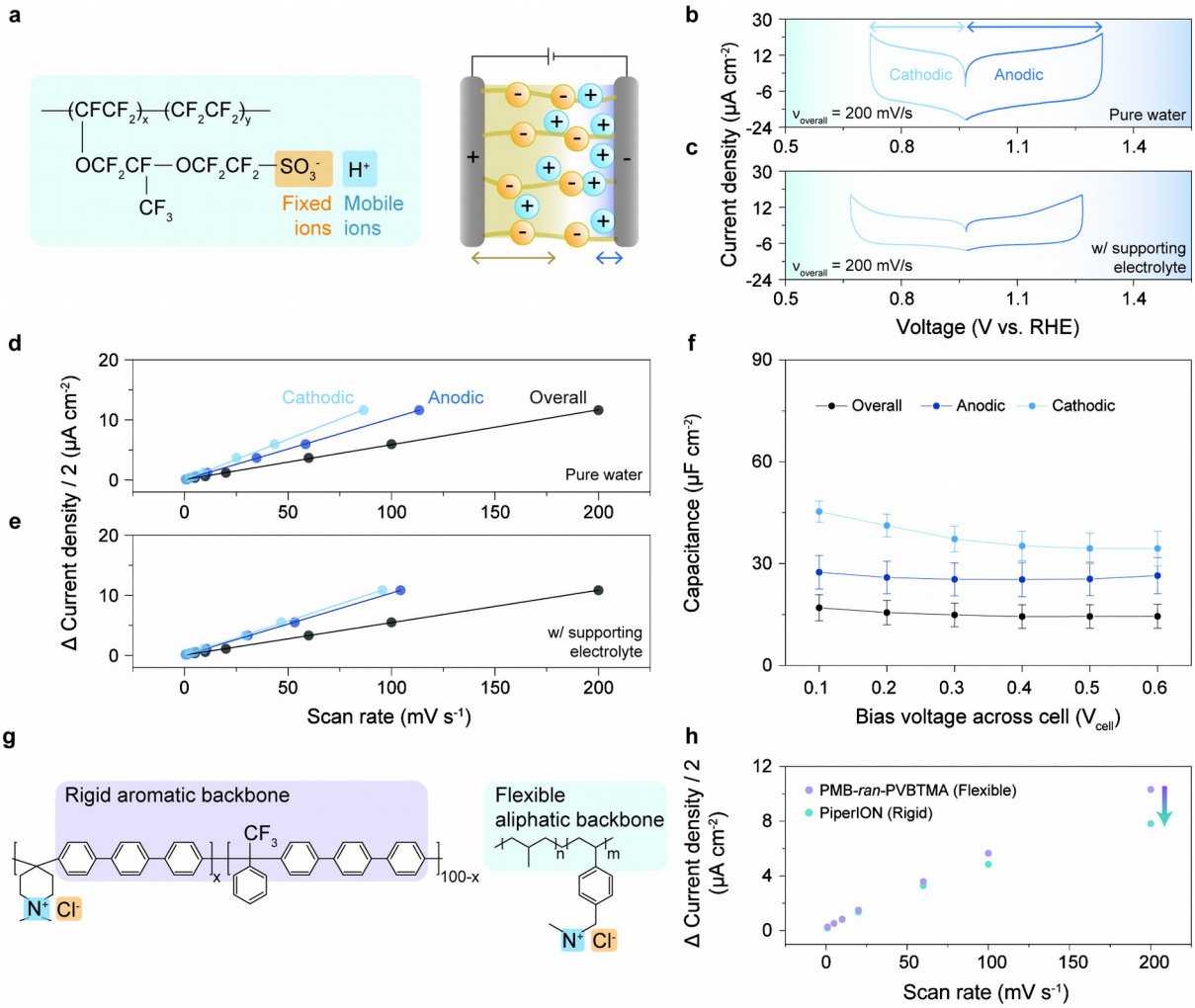


Figure 4. Interfacial charging asymmetry in Nafion CEM thin films is reversed relative to PiperION AEMs. (a) Schematic of the Nafion repeat unit, highlighting fixed sulfonate groups (SO_3^-) and mobile protons (H^+), together with an illustration of how the fixed/mobile charge configuration organizes the ionomer–electrode interface under bias. **(b, c)** Anodic and cathodic voltammograms obtained during cell-voltage sweeps at an overall scan rate of 200 mV s^{-1} using the integrated reference-electrode sensing method: (b) pure water and (c) 0.50 M H_2SO_4. The traces show the individual electrode responses resolved within the same cell-bias window. **(d, e)** Current–scan rate relationships for the overall, anodic, and cathodic responses derived from (b, c); linear fits of J versus v were used to extract C_{dl} in (d) pure water and (e) supporting electrolyte. In pure water, Nafion shows a clearer cathode/anode capacitance asymmetry, while retaining an approximately linear J–v response across the examined range. **(f)** Bias-dependent effective capacitances in pure water obtained from EIS. Impedance spectra were fit with a Randles-type circuit including a constant-phase element, and the fitted parameters were converted to Brug-corrected effective capacitances. The extracted values show a larger capacitive contribution at the cathodic H^+-dominated interface than at the anodic sulfonate-governed interface. **(g)** Chemical structures of PMB-ran-PVBTMA, with a flexible aliphatic backbone, and PiperION, with a rigid aromatic backbone. **(h)** Capacitive current density as a function of scan rate for the two anion-exchange ionomers in pure water.

2.3 Fixed-Charge Polarity and Polymer Relaxation Set the Sign and Magnitude of Ionomer Charging

To test whether the polarity of the pure-water asymmetry is set by the fixed/mobile charge configuration of the ionomer, we replaced the AEI with Nafion, a cation-exchange ionomer (CEI). In Nafion, this charge assignment is reversed relative to PiperION. Here, sulfonate groups ($-SO_3^-$) provide the fixed negative charge and protons are the mobile counterions (**Fig. 4a**). Under pure water, at a scan rate of 200 mV s^{-1}, the separated anodic and cathodic responses showed a pronounced asymmetry with the opposite polarity from that observed in PiperION (**Fig. 4b, d**). The cathodic branch exhibited a lower effective average scan rate than the anodic branch, 87 versus 113 mV s^{-1}, respectively, which corresponds to a larger apparent capacitance because $C = J/\nu$ for a given current magnitude. This result is consistent with more-effective interfacial charging when the mobile H^+ species reorganize more readily than the fixed SO_3^- framework under pure-water hydration.

Notably, Nafion retained an approximately linear current–scan rate relationship even under pure-water-fed conditions (**Fig. 4d, e**), in contrast to the PiperION AEM. For non-faradaic charging, $J = dQ/dt$; linear J–ν scaling requires the ionomer charge redistribution that compensates the electrode charge to reorganize on the time scale of the sweep. The high-rate roll-off in PiperION indicates that part of this charge response is not accessed within the scan-rate window. This behavior is consistent with QA^+ groups being tied to a rigid poly(aryl piperidinium) framework, where interfacial charge compensation requires local motion of constrained backbone and side-chain segments. In Nafion, the fixed $-SO_3^-$ groups reside on hydrated perfluorosulfonate side chains, which appear to accommodate local interfacial charge reorganization more readily over the same scan-rate range.[43,44] The different J–ν

responses, therefore, appear to reflect how readily the polymer-tethered charge environment responds to the imposed sweep, not simply the identity of the mobile counterion.[45]

Upon introduction of 0.50 M H_2SO_4, the high-rate asymmetry was reduced (**Fig. 4c, e**). The cathodic and anodic local average sweep rates shifted to 96 and 104 mV s^{-1}, respectively, which are closer than the corresponding values in pure water (87 and 113 mV s^{-1}). This narrowing indicates that dissolved electrolyte ions alleviate the interfacial charging imbalance imposed by the ionomer-defined charge environment, because mobile small ions now participate in screening at both interfaces during fast polarization. Complementary EIS measurements on CEIs reproduced the same polarity-dependent asymmetry observed in the CV analysis under pure-water hydration. On average, the cathodic capacitance was 1.46 times larger than the anodic capacitance (**Fig. 4f**), indicating a larger interfacial charging response on the H^+-dominated cathodic side than on the -SO_3^--defined anodic side.

To further probe how backbone flexibility influences pure-water EDL formation, we synthesized an anion-exchange ionomer with a flexible aliphatic main-chain architecture, in contrast to the ring-constrained framework of PiperION. Nuclear magnetic resonance (NMR) spectroscopy confirmed that the resulting poly(methylbutane-*ran*-vinylbenzyltrimethylammonium chloride) (PMB-*ran*-PVBTMA) contains a linear aliphatic backbone, with three distinct aliphatic resonances at 1.24 and 1.55–1.70 ppm assigned to backbone methylene units (**Fig. S12**). Based on its greater segmental mobility, we hypothesized that this more compliant backbone would allow interfacial charging to follow the applied bias more closely like Nafion. Consistent with this expectation, PMB-*ran*-PVBTMA implemented in the ionomer-sensing platform showed a substantially more linear J–ν relationship than the rigid aromatic PiperION in the Pt/ionomer/Pt cell (**Figs. 4g and h**).

The sum of these results shows that, in ion-exchange polymer electrolyte systems without supporting electrolyte, the physical structure of the polymer scaffold influences the time scales by which the ionomer–electrode interface reorganizes under bias (**Fig. S13**). These results identify backbone architecture, side-chain connectivity, and mechanical flexibility as important design variables for controlling interfacial charging, together with ion-exchange capacity and conductivity. A quantitative linking of these dynamics to molecular structure, however, requires more experiments, for example with temperature dependence.

These concepts could be relevant under transient or intermittent electrolysis operation, where repeated bias changes continually re-establish non-faradaic interfacial charging and relaxation, making the ionomer framework an important determinant of both the magnitude and time scale of interfacial polarization in membrane-electrode assemblies.[46,47]

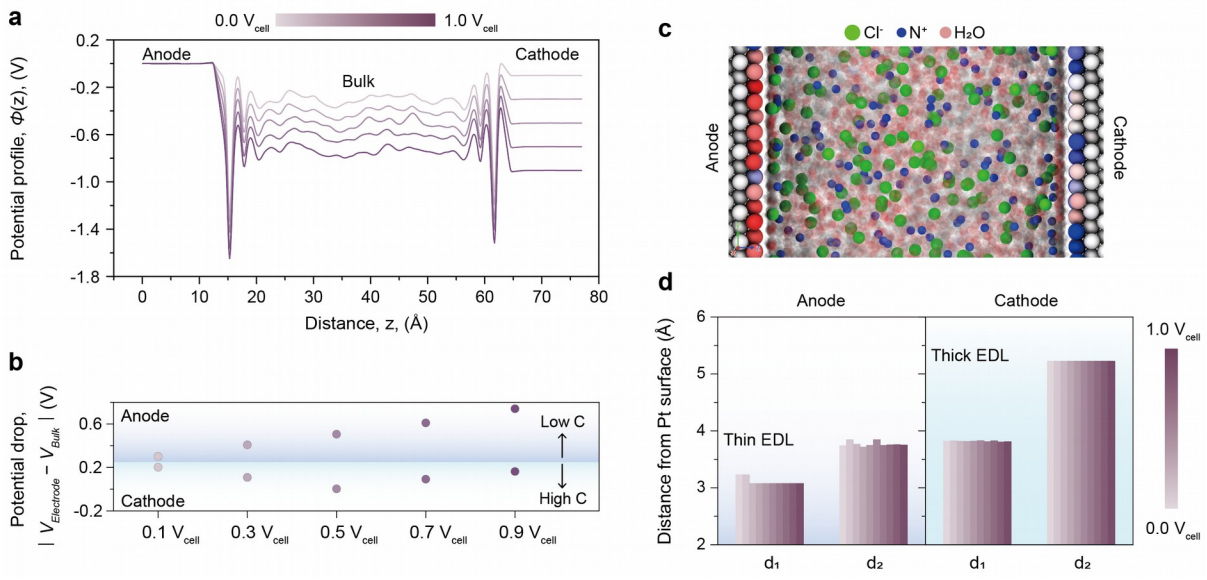


Figure 5. Molecular dynamics analysis of bias-dependent electrostatic potential partitioning and interfacial ion layering in the cell under pure-water conditions. (a) Planar-averaged electrostatic potential profiles along the surface-normal coordinate z for the Pt|PiperION|Pt model cell at applied cell voltages of 0.1, 0.3, 0.5, 0.7, and 0.9 V_{cell} under pure-water conditions. **(b)** Interfacial potential drops are extracted from (a) by defining the anodic, cathodic, and bulk ionomer potentials. The quantities $\Delta\varphi_{anode} = |\varphi_{anode} - \varphi_{bulk}|$ and $\Delta\varphi_{cathode} = |$

$\varphi_{cathode} - \varphi_{bulk}|$ quantify how the total cell voltage is partitioned between the two interfaces and provide a relative descriptor of interfacial capacitance under the series-charging condition, where a smaller local potential drop corresponds to a larger capacitance. **(c)** Representative molecular configuration of the hydrated Pt|PiperION|Pt cell used in the constant-potential MD simulation. **(d)** Bias-dependent interfacial layering distances extracted from species-resolved number-density profiles. The distances from the Pt surface to the first and second interfacial density maxima were quantified for the ion species forming the electrode-side accumulation layers over 0.1–1.0 V_{cell}.

2.4 Molecular Dynamics Simulations of Interfacial Charging in Hydrated Ionomers

To understand the origin of the capacitance asymmetry observed experimentally under pure-water conditions, we performed constant-potential MD simulations of a Pt/PiperION/Pt system hydrated with pure water under applied bias. Bias-dependent electrostatic potential profiles and species density distributions were extracted to examine how the interfacial EDL develops across the ionomer film.

To probe voltage partitioning across the fully hydrated Pt|PiperION|Pt interface under applied bias, we extracted bias-dependent electrostatic potential profiles from constant-potential MD simulations. When the full electrostatic potential profile, including the contribution of interfacial water, was analyzed, the resulting voltage partitioning was, surprisingly, *opposite* to the experimental capacitance ordering (**Fig. 5a, b**). In a series-capacitor picture, the bulk-referenced potential drop was larger at the anode than at the cathode, which would imply a larger cathodic capacitance. Because the equal-area electrodes carry equal and opposite charges under the series-charging condition, the potential-of-zero-charge-referenced interfacial potential drops provide integral-capacitance descriptors.

We therefore separated the water dipole contribution to the calculated electric-potential distribution and re-examined the voltage partitioning. In the water-excluded profiles, the experimental ordering was recovered and the potential drop was smaller at the anode and larger at the cathode, consistent with $C_{anode} > C_{cathode}$ (**Fig. S14**). This comparison

does not mean that water is absent from the real interface. Instead, the decomposition shows that interfacial-water polarization makes a major contribution to the calculated potential profile and can mask the ionic component of voltage partitioning.[48] The disagreement between the full potential profile and experiment indicates that the present classical water model does not quantitatively reproduce the measured voltage partitioning. Possible sources include the simulated charge-potential relationship and the omission of electronic polarization, charge transfer, and electron spillover at the Pt–water interface.[49-51]

To further assess ionic compactness at the two interfaces, we analyzed the N^+ and Cl^- element-density profiles over the full bias range from 0.10 to 1.0 V_{cell} (**Fig. S15**). For each electrode, we defined d_1 and d_2 as the distances from the Pt surface to the first and second ionic maxima, respectively, thereby providing a common structural descriptor of near-surface charge organization (**Fig. 5d**). At the anodic interface, both d_1 and d_2 remain shorter than the corresponding distances at the cathodic interface, indicating a more compact near-surface screening structure at the anode and a more spatially extended one at the cathode. Although these distances do not define the EDL thickness rigorously, they provide a comparative measure consistent with thinner anodic and thicker cathodic interfacial screening regions. This structural asymmetry is consistent with the experimentally observed capacitance ordering and identifies unequal ionic compactness as a key origin of the pure-water capacitance asymmetry.

3. Conclusion

We established an ionomer-sensing platform that resolves anodic and cathodic potentials in a Pt/ionomer/Pt cell with a lateral reference electrode, enabling analysis of pure-water electrochemical double layers in ionomer thin films. Using anion-exchange ionomers, we show that pure water gives rise to polarity-dependent, time- and frequency-dependent capacitance asymmetry. The mobile Cl^- at the anodic interface responds rapidly, whereas charging associated with quaternary ammonium sites relaxes more slowly. This asymmetry is suppressed by supporting electrolyte. Reversing the ionomer polarity with cation-exchange ionomers reverses the sign of the asymmetry, while comparison with a flexible aliphatic AEI shows that the magnitude of the kinetic distortion depends on how readily the polymer framework relaxes under bias. Together with molecular dynamics simulations showing that ionic screening and interfacial water polarization jointly determine voltage partitioning, these results establish that pure-water EDL formation in ionomer films is governed by fixed-charge polarity, counterion mobility, polymer segmental dynamics, and water response rather than by ion concentration alone. This framework identifies ionomer structure and local ionic environment as coupled design variables for electrode coatings and interfacial microenvironments in pure-water electrolysis and related zero-gap electrochemical devices.

Lead contact

Further information and requests for resources should be directed to and will be fulfilled by the lead contact, Shannon W. Boettcher (boettcher@berkeley.edu).

Materials availability

Commercial ionomers and reagents used in this study are available from the suppliers listed in the supplemental information. The flexible anion-exchange ionomer generated in this study can be prepared as described in the supplemental information and is available from the lead contact upon reasonable request.

Data and code availability

All data supporting the findings of this study are included within the article and its supplemental information and are also available from the authors upon request. The code used to generate the molecular dynamics structures is available at https://github.com/roncofaber/mdinterface.

Author contributions

Conceptualization, Y.K., A.D.P., W.Z., J.R., and S.W.B.; methodology, Y.K., F.R., A.D.P., W.Z., and S.W.B.; investigation, Y.K., F.R., and M.-C.K.; formal analysis, Y.K., F.R., A.D.P., W.Z., and M.-C.K.; data curation, Y.K. and F.R.; visualization, Y.K.; resources, D.P., A.M.H., J.R., and S.W.B.; writing – original draft, Y.K.; writing – review and editing, all authors; supervision, D.P., A.M.H., J.R., and S.W.B.; funding acquisition, D.P., J.R., and S.W.B.

Declaration of interests

The authors declare no competing interests.

Acknowledgments

This work was supported by the Liquid Sunlight Alliance, funded by the U.S. Department of Energy, Office of Science, Office of Basic Energy Sciences, Fuels from Sunlight Hub under Award Number DE-SC0021266, through Lawrence Berkeley National Laboratory FWP CH20LiSA under Contract No. DE-AC02-05CH11231 with the U.S. Department of Energy. The development of the ionomer-sensing platform and modeling was supported by the U.S. Department of Energy, Office of Science, Center for Ionomer-based Water Electrolysis under Award Number DE-AC02-05CH11231 and by the Multiscale Ionomer Interfacial Interrogation for Electrochemical Transformations FWP at Lawrence Berkeley National Laboratory. This work was supported by the Regional Leading Research Center (RLRC) (RS-2023-00217778) funded by the National Research Foundation (NRF) of Korea, funded by the Ministry of Science and ICT of Korea, and by the Korea Institute of Energy Technology Evaluation and Planning (KETEP) grant funded by the Ministry of Climate, Energy and Environment of the Republic of Korea (RS-2026-25540625).

References

1. Mallick, S., and Agmon, N. (2025). Multi-proton Dynamics near Membrane-water Interface. Nature Communications *16*, 3276. https://doi.org/10.1038/s41467-025-58167-w.
2. Shaikh, J., Nagarajan, A., Mitra, T., Modak, A.S., Biswas, K., Meher, G., Bhausaheb, A.J., Kannan, N.A., Sahu, B.S., Ghatak, S., et al. (2026). Membrane Interfacial Potential Governs Surface Condensation and Fibrillation of α-Synuclein in Neurons. Nature Communications *17*, 4247. https://doi.org/10.1038/s41467-026-70840-2.
3. Wei, F., Nihonyanagi, S., and Tahara, T. (2025). Elucidation of the pH-Dependent Electric Double Layer Structure at the Positively Charged Amorphous Alumina/Water Interface Using Heterodyne-Detected Vibrational Sum-Frequency Generation. Journal of the American Chemical Society *147*, 22402-22411. https://doi.org/10.1021/jacs.4c18656.
4. Ilgen, A.G., Borguet, E., Geiger, F.M., Gibbs, J.M., Grassian, V.H., Jun, Y.-S., Kabengi, N., and Kubicki, J.D. (2024). Bridging Molecular-scale Interfacial Science with Continuum-scale Models. Nature Communications *15*, 5326. https://doi.org/10.1038/s41467-024-49598-y.
5. Schott, C.M., Schneider, P.M., Song, K.-T., Yu, H., Götz, R., Haimerl, F., Gubanova, E., Zhou, J., Schmidt, T.O., Zhang, Q., et al. (2024). How to Assess and Predict Electrical Double Layer Properties. Implications for Electrocatalysis. Chemical Reviews *124*, 12391-12462. https://doi.org/10.1021/acs.chemrev.3c00806.
6. Park, W., Noh, J., An, H., Kim, J., and Chung, D.Y. (2025). Framework for Reliable Intrinsic Activity Assessment: Separating Electrical Double-Layer Capacitance and Pseudo-Capacitance in Iridium Oxide. ACS Catalysis *15*, 10938-10945. https://doi.org/10.1021/acscatal.5c01749.
7. Sebastián-Pascual, P., Herzog, A., Zhang, Y., Shao-Horn, Y., and Escudero-Escribano, M. (2025). Electrolyte Effects in Proton–electron Transfer Reactions and Implications for Renewable Fuels and Chemicals Synthesis. Nature Catalysis *8*, 986-999. https://doi.org/10.1038/s41929-025-01421-7.
8. Sebastián-Pascual, P., Shao-Horn, Y., and Escudero-Escribano, M. (2022). Toward Understanding the Role of the Electric Double Layer Structure and Electrolyte Effects on Well-defined Interfaces for

Electrocatalysis. Current Opinion in Electrochemistry *32*, 100918. https://doi.org/10.1016/j.coelec.2021.100918.
9. Fröhlich, N.L., Liu, J., Ojha, K., Hagopian, A., Doblhoff-Dier, K., and Koper, M.T.M. (2026). A Comprehensive Model for the Electric Double Layer of Stepped Platinum Electrodes. Nature Chemistry *18*, 905-912. https://doi.org/10.1038/s41557-025-02063-9.
10. Favaro, M., Jeong, B., Ross, P.N., Yano, J., Hussain, Z., Liu, Z., and Crumlin, E.J. (2016). Unravelling the Electrochemical Double Layer by Direct Probing of the Solid/Liquid Interface. Nature Communications *7*, 12695. https://doi.org/10.1038/ncomms12695.
11. Ojha, K., Doblhoff-Dier, K., and Koper, M.T.M. (2022). Double-Layer Structure of the Pt(111)–Aqueous Electrolyte Interface. Proceedings of the National Academy of Sciences *119*, e2116016119. https://doi.org/10.1073/pnas.2116016119.
12. Speelman, R., Marker, E.J., and Geiger, F.M. (2025). Quantifying Stern Layer Water Alignment Before and During the Oxygen Evolution Reaction. Science Advances *11*, eado8536. https://doi.org/10.1126/sciadv.ado8536.
13. Gunasekaran, P., Du, X., Burley, A., Le, J., Cheng, J., and Cuesta, A. (2024). Water at Electrode–electrolyte Interfaces: Combining HOD Vibrational Spectra with ab Initio-molecular Dynamics Simulations. Chemical Science *15*, 17469-17480. https://doi.org/10.1039/D4SC04766D.
14. Shibata, M.S., Morimoto, Y., Weber, A.Z., and Zenyuk, I.V. (2025). Surface Charge in Electrical Double Layer as a Kinetic Descriptor of Electrocatalytic Reactions. ACS Energy Letters *10*, 3922-3930. https://doi.org/10.1021/acsenergylett.5c01589.
15. Shibata, M.S., Morimoto, Y., Zenyuk, I.V., and Weber, A.Z. (2024). Parameter-Fitting-Free Continuum Modeling of Electric Double Layer in Aqueous Electrolyte. Journal of Chemical Theory and Computation *20*, 6184-6196. https://doi.org/10.1021/acs.jctc.4c00408.
16. Li, D., Park, E.J., Zhu, W., Shi, Q., Zhou, Y., Tian, H., Lin, Y., Serov, A., Zulevi, B., Baca, E.D., et al. (2020). Highly Quaternized Polystyrene Ionomers for High Performance Anion Exchange Membrane Water Electrolysers. Nature Energy *5*, 378-385. https://doi.org/10.1038/s41560-020-0577-x.
17. Lee, W.-H., Park, E.J., Han, J., Shin, D.W., Kim, Y.S., and Bae, C. (2017). Poly(terphenylene) Anion Exchange Membranes: The Effect of Backbone Structure on Morphology and Membrane Property. ACS Macro Letters *6*, 566-570. https://doi.org/10.1021/acsmacrolett.7b00148.
18. Hou, S., Sekar, A., Zhao, Y., Kwak, M., Oh, J., Li, K.K.-Y., Wu, P., Hannagan, R.T., Cartagena, V., Ekennia, A.C., et al. (2025). Durable, Pure Water–fed, Anion-exchange Membrane Electrolyzers through Interphase Engineering. Science *390*, 294-298. https://doi.org/10.1126/science.adw7100.
19. Foglia, F., Berrod, Q., Clancy, A.J., Smith, K., Gebel, G., Sakai, V.G., Appel, M., Zanotti, J.-M., Tyagi, M., Mahmoudi, N., et al. (2022). Disentangling Water, Ion and Polymer Dynamics in an Anion Exchange Membrane. Nature Materials *21*, 555-563. https://doi.org/10.1038/s41563-022-01197-2.
20. Brüesch, P., and Christen, T. (2004). The Electric Double Layer at a Metal Electrode in Pure Water. Journal of Applied Physics *95*, 2846-2856. https://doi.org/10.1063/1.1641517.
21. Han, S., Woo, J., Shim, J., Heo, S., Kim, S., Lee, J.Y., and Yoon, J. (2025). Advancing the Co-Based Anode Catalysts Using Ionomers in Pure-Water Anion Exchange Membrane Electrolyzers. Advanced Functional Materials *35*, 2508175. https://doi.org/10.1002/adfm.202508175.
22. Mora, J.M., Li, G., Ocon, J., and Chuang, P.-Y.A. (2025). Unraveling Alkaline Oxygen Evolution Reaction: From Ionomer Binder Materials to Electrode Engineering. ACS Applied Materials & Interfaces *17*, 48160-48172. https://doi.org/10.1021/acsami.5c06148.
23. Tricker, A.W., Lee, J.K., Babbe, F., Shin, J.R., Weber, A.Z., and Peng, X. (2023). Engineering Bipolar Interfaces for Water Electrolysis Using Earth-Abundant Anodes. ACS Energy Letters *8*, 5275-5280. https://doi.org/10.1021/acsenergylett.3c02351.
24. Ge, L., Rabiee, H., Li, M., Subramanian, S., Zheng, Y., Lee, J.H., Burdyny, T., and Wang, H. (2022). Electrochemical CO_2 Reduction in Membrane-Electrode Assemblies. Chem *8*, 663-692. https://doi.org/10.1016/j.chempr.2021.12.002.
25. Xu, H., Fang, Y., Sun, F., Wen, Y., Guo, X., and Shan, B. (2026). Cation Effect-Engineered Electrocatalytic Interfaces Boost Pure-Water CO_2 Electrolysis with Optimized Ion Dynamics. Angewandte Chemie International Edition *65*, e16321. https://doi.org/10.1002/anie.202516321.
26. Anderson, G.C., Rajupet, S., Kushner, D.I., Weber, A.Z., Radke, C.J., and Bell, A.T. (2026). Hydrogen Electrocatalysis on Perfluorosulfonic-Acid-Coated Pt. ACS Energy Letters *11*, 3435-3442. https://doi.org/10.1021/acsenergylett.6c00158.
27. Razmjooei, F., Morawietz, T., Taghizadeh, E., Hadjixenophontos, E., Mues, L., Gerle, M., Wood, B.D., Harms, C., Gago, A.S., Ansar, S.A., and Friedrich, K.A. (2021). Increasing the Performance of

an Anion-Exchange Membrane Electrolyzer Operating in Pure Water with a Nickel-based Microporous Layer. Joule *5*, 1776-1799. https://doi.org/10.1016/j.joule.2021.05.006.
28. Xu, H., Zhang, J., Eikerling, M., and Huang, J. (2024). Pure Water Splitting Driven by Overlapping Electric Double Layers. Journal of the American Chemical Society *146*, 19720-19727. https://doi.org/10.1021/jacs.4c01070.
29. Wang, Y., Narayanan, S.R., and Wu, W. (2017). Field-Assisted Splitting of Pure Water Based on Deep-Sub-Debye-Length Nanogap Electrochemical Cells. ACS Nano *11*, 8421-8428. https://doi.org/10.1021/acsnano.7b04038.
30. Lindquist, G.A., Gaitor, J.C., Thompson, W.L., Brogden, V., Noonan, K.J.T., and Boettcher, S.W. (2023). Oxidative Instability of Ionomers in Hydroxide-Exchange-Membrane Water Electrolyzers. Energy & Environmental Science *16*, 4373-4387. https://doi.org/10.1039/D3EE01293J.
31. Kusoglu, A., and Weber, A.Z. (2017). New Insights into Perfluorinated Sulfonic-Acid Ionomers. Chemical Reviews *117*, 987-1104. https://doi.org/10.1021/acs.chemrev.6b00159.
32. Xu, Q., Oener, S.Z., Lindquist, G., Jiang, H., Li, C., and Boettcher, S.W. (2021). Integrated Reference Electrodes in Anion-Exchange-Membrane Electrolyzers: Impact of Stainless-Steel Gas-Diffusion Layers and Internal Mechanical Pressure. ACS Energy Letters *6*, 305-312. https://doi.org/10.1021/acsenergylett.0c02338.
33. He, W., and Nguyen, T.V. (2004). Edge Effects on Reference Electrode Measurements in PEM Fuel Cells. Journal of The Electrochemical Society *151*, A185-A195. https://doi.org/10.1149/1.1634272.
34. Adler, S.B. (2002). Reference Electrode Placement in Thin Solid Electrolytes. Journal of The Electrochemical Society *149*, E166-E172. https://doi.org/10.1149/1.1467368.
35. Fröhlich, N.L., Eggebeen, J.J.J., and Koper, M.T.M. (2024). Measurement of the Double-layer Capacitance of Pt(111) in Acidic Conditions near the Potential of Zero Charge. Electrochimica Acta *494*, 144456. https://doi.org/10.1016/j.electacta.2024.144456.
36. Fröhlich, N.L., and Koper, M.T.M. (2025). Progress and Pitfalls in Measuring the Double-layer Capacitance of Platinum Electrodes. Current Opinion in Electrochemistry *53*, 101727. https://doi.org/10.1016/j.coelec.2025.101727.
37. Saha, P., and Zenyuk, I.V. (2021). Electric Double Layer at the Polycrystalline Platinum–Electrolyte Interface Probed by the Electrokinetic Streaming Current Method. The Journal of Physical Chemistry C *125*, 19706-19715. https://doi.org/10.1021/acs.jpcc.1c04666.
38. Bohn, L., Kieninger, J., Rupitsch, S.J., Klose, C., Vierrath, S., and Disch, J. (2024). Reference Electrode Types for Zero-Gap CO2 Electrolyzers: Benefits and Limitations. Advanced Science *11*, 2402095. https://doi.org/10.1002/advs.202402095.
39. Wang, H., and Pilon, L. (2012). Physical Interpretation of Cyclic Voltammetry for Measuring Electric Double Layer Capacitances. Electrochimica Acta *64*, 130-139. https://doi.org/10.1016/j.electacta.2011.12.118.
40. Schalenbach, M., Durmus, Y.E., Tempel, H., Kungl, H., and Eichel, R.-A. (2021). Double Layer Capacitances Analysed with Impedance Spectroscopy and Cyclic Voltammetry: Validity and Limits of the Constant Phase Element Parameterization. Physical Chemistry Chemical Physics *23*, 21097-21105. https://doi.org/10.1039/d1cp03381f.
41. Brug, G.J., van den Eeden, A.L.G., Sluyters-Rehbach, M., and Sluyters, J.H. (1984). The Analysis of Electrode Impedances Complicated by the Presence of a Constant Phase Element. Journal of Electroanalytical Chemistry and Interfacial Electrochemistry *176*, 275-295. https://doi.org/10.1016/S0022-0728(84)80324-1.
42. Merola, L., Singh, V.K., Schäfer, M., Cortese, E., Natarajan Pugazhendhi, K., Weiß, A., Qian, L., Singh, S., Benz, S.L., Sann, J., et al. (2026). Triple-Phase Boundary Instability as a Key Degradation Factor in Sulfide|(oxy)halide Dual-Electrolyte Solid-State Batteries. Joule *10*, 102444. https://doi.org/10.1016/j.joule.2026.102444.
43. Masuda, T., Ikeda, K., and Uosaki, K. (2013). Potential-Dependent Adsorption/Desorption Behavior of Perfluorosulfonated Ionomer on a Gold Electrode Surface Studied by Cyclic Voltammetry, Electrochemical Quartz Microbalance, and Electrochemical Atomic Force Microscopy. Langmuir *29*, 2420-2426. https://doi.org/10.1021/la304705k.
44. Katzenberg, A., Mukherjee, D., Dudenas, P.J., Okamoto, Y., Kusoglu, A., and Modestino, M.A. (2020). Dynamic Emergence of Nanostructure and Transport Properties in Perfluorinated Sulfonic Acid Ionomers. Macromolecules *53*, 8519-8528. https://doi.org/10.1021/acs.macromol.0c01213.
45. Kusoglu, A., Vezzù, K., Hegde, G.A., Nawn, G., Motz, A.R., Sarode, H.N., Haugen, G.M., Yang, Y., Seifert, S., Yandrasits, M.A., et al. (2020). Transport and Morphology of a Proton Exchange Membrane

Based on a Doubly Functionalized Perfluorosulfonic Imide Side Chain Perflourinated Polymer. Chemistry of Materials *32*, 38-59. https://doi.org/10.1021/acs.chemmater.8b05012.
46. Gankhuyag, T., Obata, K., and Takanabe, K. (2025). Potential Regulation for Stable Electrocatalysts in Alkaline Water Electrolyzers during Dynamic On and Off Operation through Double-Layer Capacitance Engineering. The Journal of Physical Chemistry C *129*, 18043-18050. https://doi.org/10.1021/acs.jpcc.5c04643.
47. Rocha, F., and Proost, J. (2021). Discriminating Between the Effect of Pulse Width and Duty Cycle on the Hydrogen Generation Performance of 3-D Electrodes during Pulsed Water Electrolysis. International Journal of Hydrogen Energy *46*, 28925-28935. https://doi.org/10.1016/j.ijhydene.2020.11.232.
48. Limaye, A., Suvlu, D., and Willard, A.P. (2024). Water Molecules Mute the Dependence of the Double-Layer Potential Profile on Ionic Strength. Faraday Discussions *249*, 267-288. https://doi.org/10.1039/d3fd00114h.
49. Li, L., Reuter, K., and Hörmann, N.G. (2025). Deciphering the Capacitance of the Pt(111)/Water Interface: A Micro- to Mesoscopic Investigation by AIMD and Implicit Solvation. ACS Electrochemistry *1*, 186-194. https://doi.org/10.1021/acselectrochem.4c00062.
50. Mohandas, N., Bawari, S., Shibuya, J.J.T., Ghosh, S., Mondal, J., Narayanan, T.N., and Cuesta, A. (2024). Understanding Electrochemical Interfaces through Comparing Experimental and Computational Charge Density–Potential Curves. Chemical Science *15*, 6643-6660. https://doi.org/10.1039/d4sc00746h.
51. Li, L., Eggert, T., Reuter, K., and Hörmann, N.G. (2025). Electron Spillover into Water Layers: A Quantum Leap in Understanding Capacitance Behavior. Journal of the American Chemical Society *147*, 22778-22784. https://doi.org/10.1021/jacs.5c04728.